Acta Crystallographica Section A
Foundations of Crystallography
ISSN 0108-7673

Received 4 May 2011
Accepted 2 September 2011

Form, symmetry and packing of biomacromolecules. V. Shells with boundaries at anti-nodes of resonant vibrations in icosahedral RNA viruses

A. Janner

Theoretical Physics, FNWI, Radboud University, Heyendaalseweg 135, NL-6525 AJ Nijmegen, The Netherlands. Correspondence e-mail: a.janner@science.ru.nl

The RNA viruses cowpea chlorotic mottle, satellite tobacco mosaic, pariacoto and MS2, already considered in part IV of this series of papers [Janner, A. (2011*a*), *Acta Cryst.* A**67**, 517–520], are investigated further, with the aim to arrive at a possible physical basis for their structural properties. The shell structure of the filled capsid is analyzed in terms of successive spherical boundaries of the sets of icosahedral equivalent chains. By inversion in the sphere enclosing the capsid, the internal boundaries are transformed into external ones, which are more easily visualized. This graphical procedure reveals the presence of regularly spaced shells with boundaries fitting with anti-nodal surfaces of the virus considered as an elastic resonator. The centers of gravity of the various chains occur in the nodal regions of eigenvibrations with wavelength $\lambda = R_0/K_0$, where R_0 is the radius of the virus and K_0 takes one of the values 12, 6, 4, 3, depending on the mode. The resonator model is consistent with practically all spherical shell boundaries, whereas deviations are observed for the icosahedral axial modes, which apparently play a secondary role with respect to the spherical ones. Both the spherical and the axial anti-nodal surfaces fit very well with the packed structure of the viruses in the crystal which, accordingly, is expected to have eigenfrequencies related to those of the virus. These results open the way to a better understanding of the possibility of breaking the capsid using resonant forced oscillations excited, for example, by an applied elastic shock or by irradiation with femtosecond laser pulses, as already realised by K.-T. Tsen and co-workers. An alternative 'plywood' model connected to the extreme elastic properties of the capsid is also considered.

1. Introduction

The pariacoto virus [refcode 1f8v of the Brookhaven Protein Data Bank (PDB), with primary reference Tang *et al.* (2001)], the satellite tobacco mosaic virus/RNA complex (PDB refcode 1a34; Larson *et al.*, 1998), the native cowpea chlorotic mottle virus (PDB refcode 1cwp; Speir *et al.*, 1995) and the RNA MS2 bacteriophage (PDB refcode 1zdh; Valegård *et al.*, 1997), already considered in part IV (Janner, 2011*a*), are investigated further in an attempt to connect the geometry of their structure with physical properties. The interest in these viruses has been stimulated by the work of Twarock and Keef of the York Center for Complex System Analysis, York, and by that of Stockley, Astbury Center for Structural Molecular Biology, Leeds (Jonoska & Twarock, 2006; Toropova *et al.*, 2008; Keef & Twarock, 2009*a*,*b*; Grayson *et al.*, 2009; Stockley & Twarock, 2009; Keef *et al.*, 2011).

As verified in part IV, these four viruses have the same generic structural properties of several other viruses, like crystallographic scaling, indexed forms enclosing axial-symmetric clusters of chains, and a crystal packing which reflects features of the individual virus. Moreover, these phenomenological laws, derived by the author in previous publications devoted to axial-symmetric biomacromolecules and extended to icosahedral viruses, apply equally well to the various ordered components of the capsid and of the genome.

Here the enclosing forms of capsid and genome are considered in the spherical symmetry approximation instead of in terms of indexed icosahedral forms. In a similar way, the axial-symmetric cases are handled by corresponding cylindrical forms. The combination of external and internal boundaries of these forms leads to spherical and cylindrical shells.

In publications of other authors, spherical shells have been considered in connection with the extreme elastic properties of the capsid which lead to conformal changes, like buckling and swelling transitions in viral maturation [see, for example, Tama & Brooks, 2005; Jonoska & Twarock, 2006; Klug *et al.*, 2006; Guérin & Bruinsma, 2007; Bünemann, 2008, and references therein].

For the two-dimensional figure visualization a projection from the three-dimensional structure has been adopted. This has the drawback of hiding the boundaries of the internal spherical shells. Therefore, in §2, the internal shell boundaries of the various chain polymers are visualized by applying a sphere inversion transformation (Coxeter, 1961), which turns the virus inside out. The striking result is that the shell boundaries occur at the surface of equally spaced spheres.

One then verifies in §3 that this spacing fits with the crystal packing of the virus, in a way consistent with the packing lattice Λ_P, introduced in part I (Janner, 2010*a*) and discussed further in part III (Janner, 2011*b*). We recall that the packing lattice Λ_P is a three-dimensional lattice invariant with respect to the space group of the crystal as packing of equal spheres, which has the crystal lattice Λ as a sublattice. Moreover, the centers of the spheres and their kissing points (where the spheres touch) are points of Λ_P. This correspondence supports the view, already pointed out in part II for the serotypes of the rhinovirus (Janner, 2010*b*), that there is an intimate connection between the detailed structure of a single virus and the space-group symmetry of its crystal.

The existence of enclosing forms of axial-symmetric clusters of monomers with vertices at (projected) points of a lattice with the same point group symmetry (the form lattice Λ_F) suggests considering cylindrical shells around the two-fold, three-fold and five-fold icosahedral axes, as carried out in §4. Again the observed shell boundaries are at equally spaced cylinders, oriented along the symmetry axis, having the same inter-space distance as in the set of spherical shells. The situation recalls the diagrammatic representation of the packing forms found in the light harvesting protein LH2 and in the rhodopsin retinal complex [see Figs. 14 and 15 of Janner (2010*a*)].

In §5 an attempt is made to arrive at a possible physical interpretation of the shell boundaries as anti-nodal surfaces of viral eigenvibrations. Considered is the possibility of viral destruction by means of resonant forced oscillations. Some final remarks conclude the paper. The way the results have been obtained is commented on from a general point of view in Appendix *A*.

2. Spherical viral shells

2.1. General aspects

Inversion in a sphere with center O and radius R_0 transforms any point P (not equal to O) in the inverted point P' on the ray OP with distance OP' from O satisfying the relation

$$\mathbf{OP} \times \mathbf{OP}' = R_0^2, \tag{1}$$

where $\mathbf{OP}$ and $\mathbf{OP}'$ are position vectors along the same ray. This inversion transforms spheres into spheres, conserves the point group symmetry and leaves invariant the sphere of radius R_0, denoted as the *invariant sphere* (Coxeter, 1961).

The center of the inversion transformations considered is the center of the virus. In the inverted viral structure the atomic positions inside the invariant sphere are mapped to outside points, and conversely. Note that the inverted structure depends on R_0.

An optimal choice of R_0 should lead to simple relations between R_0 and the various shell boundaries taking into account the three symmetry groups involved: the rotation group $SO(3)$, the icosahedral point group 235 and the space group of the crystal.

This is indeed the case if one chooses the external spherical boundary of the capsid (with radius R_e) as the invariant sphere ($R_0 = R_e$), not necessarily the one with maximal radius, but possibly one excluding protruding elements, like external loops and/or terminal chain segments. The radius of the sphere enclosing these (external) protruding elements is denoted as R_{pe}.

In a similar way, one distinguishes between an internal boundary of the capsid, with radius R_i, and the boundary of the internal protruding elements (directed towards the center), with radius R_{pi} for each of the icosahedral chain subsystems. Thus for each of the protein chains involved (say A), one has main external and internal shell boundaries $R_e(A)$, $R_i(A)$ and possibly protruding ones $R_{pe}(A)$ and $R_{pi}(A)$, respectively. The same approach is applied to the RNA chains, where of course protruding shells do not occur.

2.2. Observed shell boundaries

Applying to the four viruses listed in the *Introduction* the inversion in a sphere as a graphical tool for the visualization of the internal boundaries of a given external spherical one, one arrives at the amazing general result:

For any of the ordered chains of the capsid and of the genome of these four viruses, whose coordinates are listed in the structural data of the PDB files, the shell boundaries (main and/or protruded) occur at the surface of spheres with radius R satisfying the condition

$$R = k\,R_0/K_0, \tag{2}$$

where R_0 is the radius of the chosen invariant inversion sphere, k is an integer and $K_0 = 12$. The numerical value 12 is an empirical unexpected result. Accordingly, the possible spherical shell boundaries are equidistant, with an inter-sphere distance d given by

$$d = R_0/12, \tag{3}$$

so that their radius, expressed in units of d, takes the value of the integer k. Moreover, the k value of the external boundary of the genome is equal to that of the main internal boundary of the capsid, whereas the internal protruding shell of the same capsid interacts directly with the genome. This justifies the distinction made between main and protruded boundaries.

Of course, as always, the experimental value of a given radius is an approximation of the ideal one. The graphical representation of the structure together with the shell boundaries involved allows a visual estimation of the difference between real and ideal.

Table 1 indicates for each of the four viruses the value of the radius R_0 and the type, label and length of the chains which build the shells. In all cases the invariant sphere has the same

Table 1
Molecular description.

The length gives the number of backbone positions determined.

PDB	RNA virus	Radius R_0 (Å)	Chains	Type	Length
1cwp	Cowpea chlorotic mottle virus	134.30	*A*, *B*, *C*	Coat proteins	190
			D, *F*	RNA	4
			E	RNA	2
1a34	Satellite tobacco mosaic virus	85.75	*A*	Capsid protein	151
			B	RNA	10
			C	RNA	10
1zdh	Bacteriophage MS2	132.7	*A*, *B*, *C*	Coat protein	355
			R, *S*	RNA	19
1f8v	Pariacoto virus	155.30	*A*, *B*, *C*	Coat protein β	355
			D, *E*, *F*	Coat protein γ	40
			R	RNA	25

radius as the (main) external boundary of the capsid which, in the present case and in units of d, is given by $R_0 = R_e = 12$. The radii of the other shell boundaries are then deduced from plots of the direct and inverse chain structures. The result is summarized in Table 2. Corresponding figures, supplemented by a short comment, are indicated for each of the viruses considered.

Cowpea chlorotic mottle virus. The boundaries of the three coat proteins A, B, C are practically the same so that they form a single shell with negligible protruding elements (Fig. 1, left-hand side). The ordered segments D, E, F of the RNA chains also form a single shell (Fig. 1, right-hand side). Actually, E is so short that it can be neglected.

Satellite tobacco mosaic virus. Loops and chain terminals of the coat protein A which protrude the internal (main) boundary of the capsid form their own shell with unit width d (Fig. 2, left-hand side). The internal boundary of the RNA shell has a slightly larger radius than the ideal one given by $k = 6$, *i.e.* 43.7 Å instead of 42.7 Å (Fig. 2, right-hand side).

In this virus one finds the intriguing single case of SO_4^{2-} ions at positions which, when transformed by inversion in the sphere inscribed in the enclosing viral form, coincide with the icosahedral vertices of the external ico-dodecahedron (not shown).

Bacteriophage MS2. While the three coat proteins A, B, C form a single shell delimited by $R_e(A, B, C) = 12$ and $R_i(A, B, C) = 10$ (in units of d), with negligible protruding elements, only the external RNA boundary is the same for the two chains R, S. The internal boundary of these chains differs by one unit: $R_i(R) = 8$ and $R_i(S) = 9$ (Fig. 3).

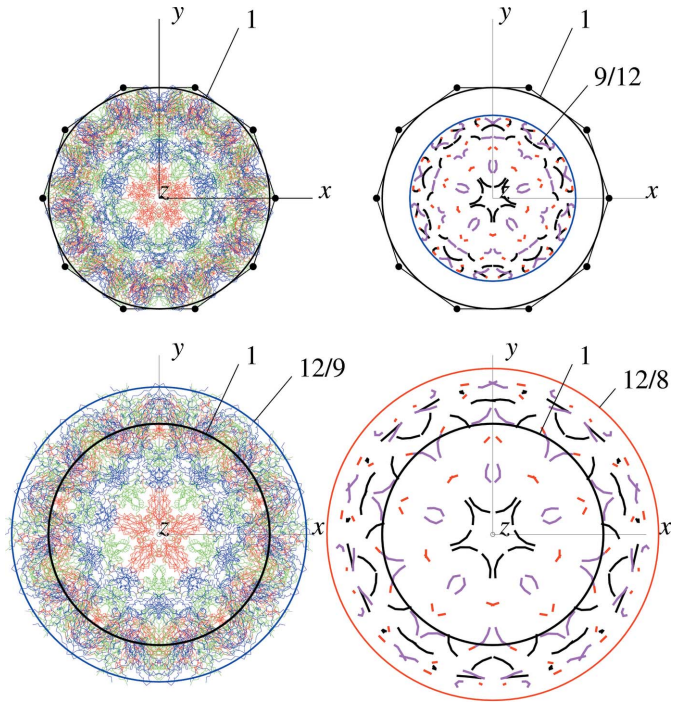

Figure 1
The direct (upper part) and inverted (lower part) structures of the capsid (on the left-hand side) with the coat proteins A (red), B (green), C (blue) and of the genome (on the right-hand side) with the RNA chains D (black), E (red), F (magenta) of the cowpea chlorotic mottle virus are shown in a projection along the five-fold axis. The radii of the shell boundaries are indicated in units of the radius R_0 of the invariant sphere, chosen equal to the size of the virus, enclosed in an ico-dodecahedron with vertices indicated by black dots. Note that the internal boundary of the capsid [at $R_i(A, B, C) = 9R_0/12$] coincides with the external one $R_e(D, E, F)$ of the genome, whereas its internal one is $R_i(D, E, F) = 8R_0/12$. Only the invariant sphere is indicated together with the external boundaries, not the internal ones.

Pariacoto virus. As already pointed out, the RNA duplex is wrapped around a dodecahedron scaled by a factor $1/\tau$ with respect to the ico-dodecahedron enclosing the capsid. Despite this special symmetry relation, its shell obeys the same general laws as in the other viruses. In the present case one has $R_e(R) = 9$ and $R_i(R) = 7$ (Fig. 4, right-hand side). The shell structure of the six different capsid proteins (A, B, C, D, E, F) is fairly rich with external and internal main and protruded boundaries. For A, B, C, the so-called β proteins, the boundaries are practically at ideal positions (Fig. 4, left-hand side). Those of the γ proteins D, E, F show small deviations from the ideal

Table 2
Spherical shell boundaries (with radii in units of $d = R_0/12$).

Virus		Capsid shell boundaries		Genome shell boundaries	
		External	Internal	External	Internal
Cowpea	Main	$R_e(A, B, C) = 12$	$R_i(A, B, C) = 9$	$R_e(D, F) = 9$	$R_i(D, F) = 8$
Tobacco	Main	$R_e(A) = 12$	$R_i(A) = 9$	$R_e(B, C) = 9$	$R_i(B, C) = 6$
	Protruded		$R_{pi}(A) = 8$		
MS2 bacteriophage	Main	$R_e(A, B, C) = 12$	$R_i(A, B, C) = 10$	$R_e(R, S) = 10$	$R_i(R) = 8$, $R_i(S) = 9$
Pariacoto	Main	$R_e(A, B, C) = 12$	$R_i(A, B, C) = 9$	$R_e(R) = 9$	$R_i(R) = 7$
		$R_e(D) = 10$	$R_i(D) = 9$		
		$R_e(E, F) = 9$	$R_i(E, F) = 8$		
	Protruded	$R_{pe}(A, B, C) = 13$	$R_{pi}(A, B, C) = 8$		

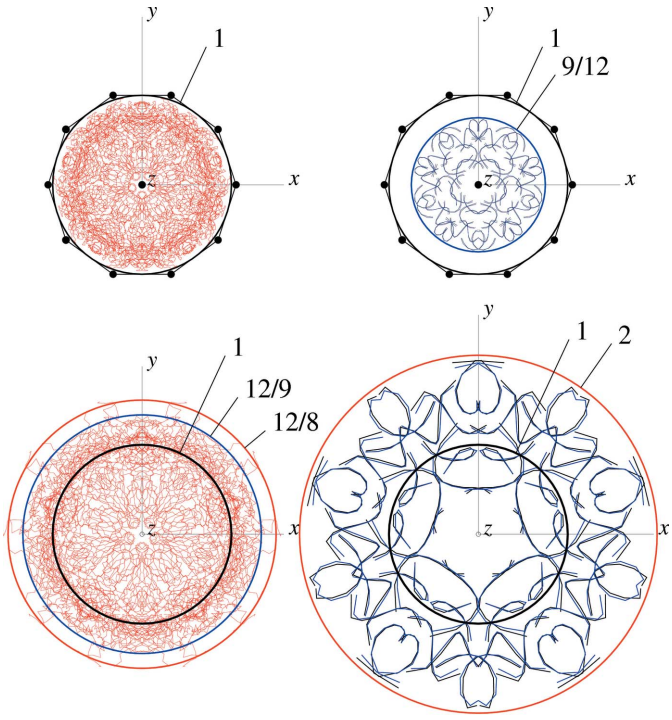

Figure 2
The boundaries of the spherical shells of the satellite tobacco mosaic virus are indicated in a similar way as in the previous figure. Now, the coat protein A (red) forms two shells, a main one between $R_e(A) = R_0$ and $R_i(A) = 9R_0/12$ and a protruded one between $R_i(A)$ and $R_{pi}(A) = 8R_0/12$. The protruded shell overlaps the single RNA shell formed by the two chains B (black), C (blue), both delimited by $R_e(B, C) = 9R_0/12$ and $R_i(B, C) = R_0/2$.

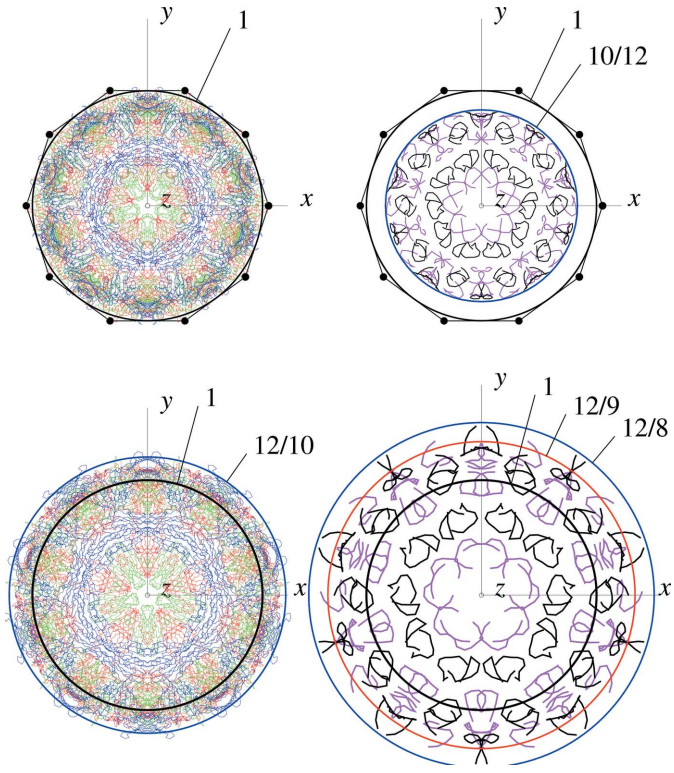

Figure 3
The shell structure of the MS2 bacteriophage is shown in a similar way as in the previous two figures. The shell boundaries of the coat proteins A (red), B (green), C (blue) are at $R_e(A, B, C) = R_0$ and $R_i(A, B, C) = 10R_0/12$. Few loops protruding the internal boundary $R_i(A, B, C)$, without defining an own shell, interact with the RNA chains R (magenta), S (black) with external radius $R_e(R, S) = R_i(A, B, C)$. The internal boundaries of these two chains are different: $R_i(S) = 9R_0/12$ and $R_i(R) = 8R_0/12$.

values (not shown). Their length is much shorter than for the β chain (40 residues instead of 355) and this hints at less order.

Taken as an isolated case, the unit width of the protruded shells of the pariacoto capsid (Fig. 4) seems to be accidental. It appears as non-accidental when one also considers the octahedral cage of the sulfur oxygenase reductase SOR, where the chimney-like protrusions also have a unit height, equal to that of the cubic elementary cell of the form lattice [see Fig. 1(*b*) of Janner (2008)].

3. Crystal spherical packing

The serotype differentiation of human rhinoviruses has been shown to be related to the packing of these viruses in the crystal (Janner, 2010*b*). The investigation revealed close connections between properties of the individual virus and its space-group symmetry. It is, therefore, natural to try to describe the crystal packing in terms of the equidistant set of spheres considered in the previous section.

It is agreeable to verify that what one expects is indeed realised. In the four viruses considered, the spherical shell structure, properly extended outside the virus, fits very well with the crystal packing. This is shown in Fig. 5 for the MS2 bacteriophage (compare this figure with Fig. 5 of part IV) and in Fig. 6 for the cowpea chlorotic mottle virus. The corresponding figures of the satellite tobacco mosaic virus and of the pariacoto virus (not shown here) are similar.

From these figures it follows that the parameters a, b, c of the crystal lattice Λ can be expressed in units of the sphere inter-spacing d. For example, for the MS2 virus one deduces from Fig. 5 the relations

$$a = 6u = 26d, \qquad b = 6v = 26d, \qquad c = 15w = 60d, \quad (4)$$

where u, v, w are the parameters of the packing lattice Λ_P, also expressible in units of d,

$$u = v = (13/3)d, \qquad w = 4d. \quad (5)$$

This type of correspondence is reported in Table 3 for all the four viruses considered. From the table, one easily obtains the ratios of the crystal lattice parameters which, because of their rational value when expressed in units of d, imply that (in the ideal case at least and, for the pariacoto virus, in the orthorhombic approximation of its lattice Λ) the crystal lattices are integral (Janner, 2004). The corresponding reduction of independent structural parameters from the orthorhombic a, b, c and the hexagonal a, c to the single d one is typical for strongly correlated systems (Janner, 2005*a*,*b*,*c*). The comparison with the experimental values follows directly from the data specified in Table 3.

Table 3
Crystal packing parameters.

PDB	Virus	Space group	Unit width $d = R_0/12$ (Å)	Crystal lattice parameters a, b, c			
					In Å	In Λ_P parameters u, v, w	In d unit width
1cwp	Cowpea virus	$P2_12_12_1$	11.19	a	381.30	$8u$	$(104/3)d$
				b	381.30	$8v$	$(104/3)d$
				c	408.66	$9w$	$39d$
1a34	Tobacco virus	$I222$	7.15	a	174.27	$16u$	$24d$
				b	191.77	$18v$	$27d$
				c	202.50	$19w$	$22d$
1zdh	MS2 bacteriphage	$H32$	11.06	a	288.00	$6u$	$26d$
				b	288.00	$8v$	$26d$
				c	653.00	$15w$	$32d$
1f8v	Pariacoto virus	$P12_11$ ($\beta = 90.93$)	12.94	a	329.33	$12u$	$25d$
				b	346.94	$13v$	$26d$
				c	424.89	$16w$	$60d$

4. Axial symmetric shells

In addition to the rotation group and the crystal space group considered in the previous two sections, the third relevant group is the icosahedral one with the corresponding two-fold, three-fold and five-fold symmetry axes.

The 60 icosahedral equivalent chains are, accordingly, partitioned into tetrameric, hexameric and decameric clusters with orthorhombic, trigonal and pentagonal symmetry, respectively.

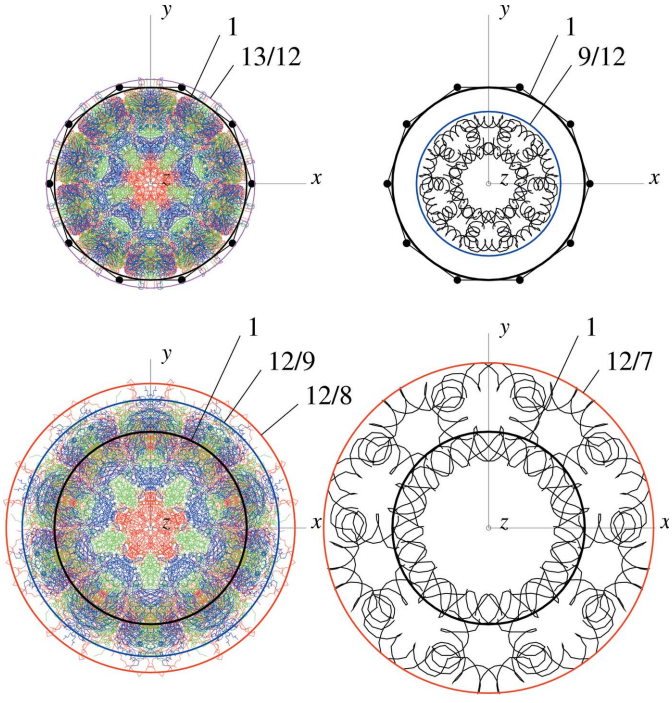

Figure 4
The structure of the spherical shells in the pariacoto virus is plotted in a similar way as in previous figures. The coat proteins A (red), B (green), C (blue) form a main shell [between $R_e(A, B, C) = R_0$ and $R_i(A, B, C) = 9R_0/12$] and two protruded shells: an external one [with $R_{pe}(A, B, C) = 13R_0/12$] and an internal one [with $R_{pi}(A, B, C) = 8R_0/12$] which overlaps the external part of the RNA chain R (black) [with $R_e(R) = 9R_0/12$]. The internal shell boundary of the R chain is at $R_i(R) = 7R_0/12$.

In analogy with the spherical shells, one expects that these clusters are enclosed in axial shells, with boundaries at equidistant cylindrical surfaces. Moreover, in order to be consistent with the spherical shell structure, the same unit distance d should occur along and perpendicular to the axial directions, with cylindric radii R and height H obeying the relations

$$R = k_R d, \qquad H = k_H d, \qquad k_R,\ k_H \text{ integers}, \tag{6}$$

where $d = R_0/12$ as in equation (3).

A systematic verification of the validity of this equation requires, for each chain of the four viruses, 31 different cases

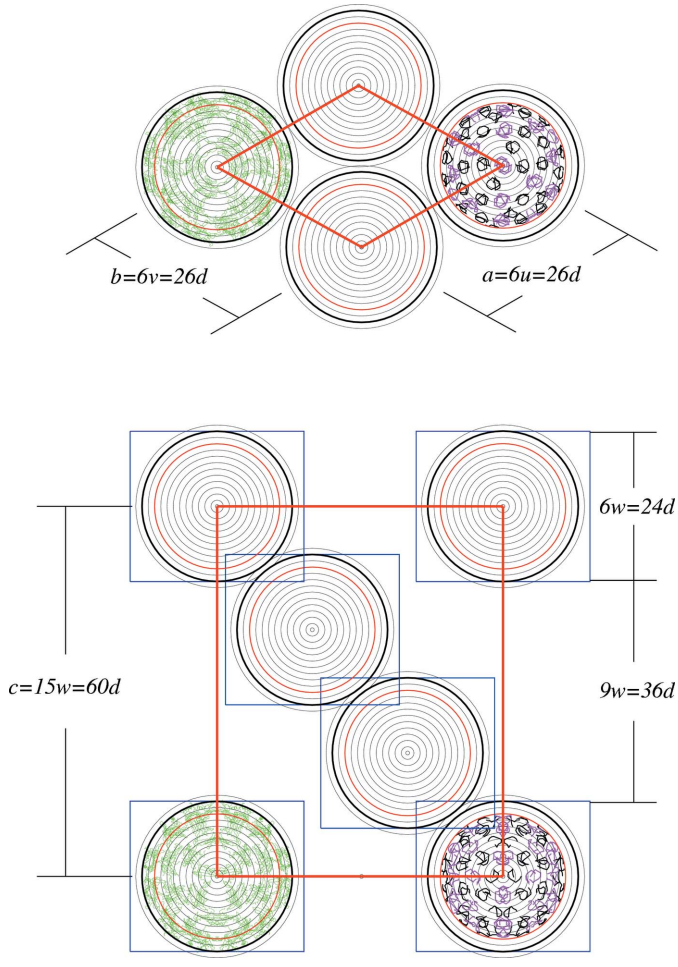

Figure 5
The shell structure of the MS2 bacteriophage is compatible with the packing of the virus in the crystal. Enhanced, by a thick black line, is the invariant sphere with the radius R_0 which corresponds to the size of the virus and coincides with the external boundary of the shell belonging to the coat proteins A (shown in green), B, C (not shown). The enclosing boundary of the RNA chains R (magenta), S (black) is plotted in red. Indicated are the rational relations between the parameters a, b, c of the crystal lattice Λ and the parameters u, v, w of the packing lattice Λ_P, also expressed rationally in terms of the single inter-spherical distance $d = R_0/12$. Accordingly, Λ and Λ_P are integral lattices.

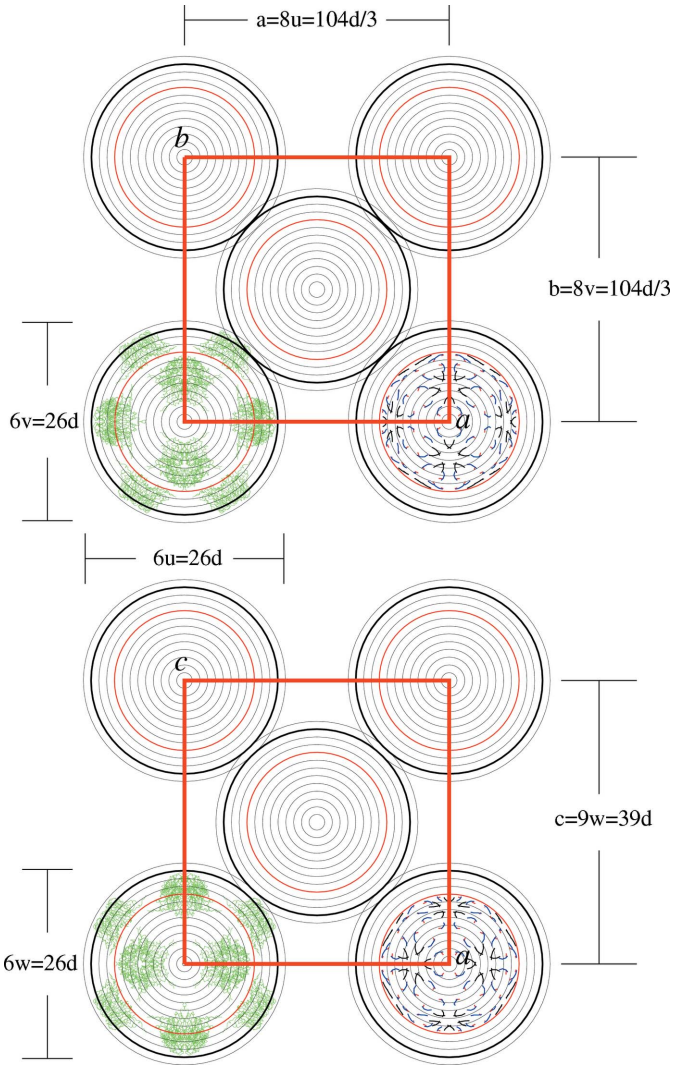

Figure 6
Similar representation as in the previous figure of the shell structure of the cowpea chlorotic mottle virus in relation to its crystal packing. The parameters of the crystal lattice Λ are expressed in terms of those of the packing lattice Λ_P and related to the inter-spherical distance $d = R_0/12$, where now R_0 is the radius of the cowpea chlorotic mottle virus. Again, Λ and Λ_P are integral lattices. Shown is a filling by the coat protein A (green) and by the RNA chains D (black), E (red), F (blue).

according to the 15 tetrameric, the ten hexameric and the six decameric clusters, respectively. This systematic investigation has only been made for the A coat protein and the RNA chain R of the pariacoto virus. The result is summarized in Tables 4, 5 and 6 in terms of the radial and axial k-values of the shells with boundaries denoted by R_e, R_i and H_e, H_i for the external and internal radial and axial ones, respectively. The meaning of 'external' and 'internal' in the radial plane is the natural one, whereas H_e denotes the height along the axial direction of the boundary furthest away from the equatorial plane, H_i being that of the other limiting boundary of the same shell. In Tables 4, 5 and 6 the additional intermediate boundaries R_{pe}, R_{pi} and H_{pe}, H_{pi}, which, respectively, delimit main from protruded segments of the coat proteins, are also given.

From this check for the observed axial shells one finds a global validity only of equation (6). In particular, a question mark indicates the cases where the assignment of specific k_R and k_H values is not evident from the graphical plot.

One observes similar situations by sampling additional chains in the pariacoto and in the other viruses. Three illustrative examples are shown: in Fig. 7 a three-fold hexamer of the A, B, C chains in the satellite tobacco mosaic virus, in Fig. 8 a five-fold decamer of the A coat protein and of the RNA chain R in the pariacoto virus, and in Fig. 9 a two-fold RNA tetramer of these chains in the same virus. In all these figures the coat proteins are plotted on the left-hand side and the RNA chains on the right-hand side.

Finally, Fig. 10 demonstrates for the pariacoto virus the compatibility of the axial tetrameric shells belonging to the chains A, D, E, F and R, labeled as {5, 24, 51, 56}, with the monoclinic (almost orthorhombic) crystal structure.

Concluding, the axial symmetric shells postulated in equation (6) represent a secondary feature only, even if compatible with the spherical shells which can be considered as a dominant structural phenomenon in the four viruses. Both types of shells, properly extended outside the viral boundary, fit very well with the crystal packing.

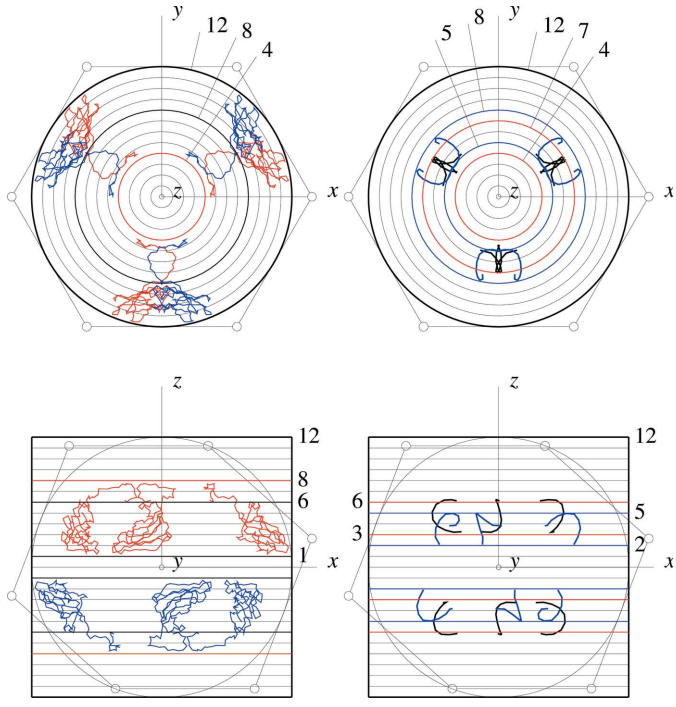

Figure 7
Axial shell structure of the hexamer {5, 25, 45; 11, 31, 41} of the satellite tobacco mosaic virus. Plotted are the chains of the coat protein A (on the left-hand side, with the two trimers in red and in blue) and of the RNA chains B (black) and C (blue) on the right-hand side, in a projection along and perpendicular to the rotation three-fold axis. Indicated are the k values of the various shells boundaries (colored lines) in units of the inter-spacing distance $d = R_0/12$ (in the rotation plane and along the axis, respectively). The cylinder enclosing the virus has radius $R_0 = 12d$ and height $H_0 = 2R_0$ (thick black line). For the protein A note the splitting into a protruding shell [delimited by (4, 8) for k_R and (6, 8) for k_H] and a main shell [delimited by (8, 12) for k_R and (1, 6) for k_H]. The two RNA chains B, C are each enclosed in their own shell, delimited by (8, 5) and (7, 4) for k_R and by (6, 3) and (5, 2) for k_H.

Table 4
Pariacoto virus: two-fold axial symmetric shells.

Radii and heights are in units of $d = R_0/12$.

	Capsid coat protein *A*								RNA chain *R*			
Tetrameric clusters	R_{pe}	R_e	R_i	R_{pi}	H_{pe}	H_e	H_i	H_{pi}	R_e	R_i	H_e	H_i
{0, 32, 37, 46}		12	9	7	6	4	0		8	6	5	3
{1, 33, 38, 47}		12	9	7	5	4	0		8	6	6	3
{2, 34, 39, 48}		10	7	6	10	9	6	5	7 (?)	2	8	5
{3, 30, 35, 49}		6	2	1	13	12	9	8	3	0	9 (?)	7
{4, 31, 36, 45}		10	7	4	10	9	6	5	3	0	9 (?)	7
{5, 24, 51, 56}	11	9	6 (?)			10	7	3	8	6	5	3
{6, 20, 52, 57}	12	11	8	7		7	3		8	6 (?)	4	0
{7, 21, 53, 58}	13	12	7			7	4	0	9	6	4	0
{8, 22, 54, 59}	11	9	6			10	6	4	8	6	5	2
{9, 23, 50, 55}		13 (?)	9	8	3	2	−2	−3	9 (?)	7	3 (?)	−3 (?)
{10, 15, 29, 43}	13	12	9	8	6	2	0		9	7	1	−1
{11, 16, 25, 44}	13	13	9	8		4	0		9	6	5	1
{12, 17, 26, 40}	8	7	4			11	8	6	7	3	7	5
{13, 18, 27, 41}	8	7	4	3		11	7 (?)		7	3 (?)	8	5
{14, 19, 28, 42}	13	12	9	7	5	2	0		8	6	5	2

Table 5
Pariacoto virus: three-fold axial symmetric shells.

Radii and heights are in units of $d = R_0/12$.

	Capsid coat protein *A*								RNA chain *R*			
Hexameric clusters	R_{pe}	R_e	R_i	R_{pi}	H_{pe}	H_e	H_i	H_{pi}	R_e	R_i	H_e	H_i
{0, 9, 22; 32, 50, 59}		7	3			12	8	7	5	1	8	6
{1, 5, 23; 33, 51, 55}		7	4	0	12	11	7	8	5	1	9	6
{2, 6, 24; 34, 52, 56}		12	9	6	7	8	5		9	6	7 (?)	3
{3, 7, 20; 30, 53, 57}		13	9	8	4	2	−2		8	6	4	2
{4, 8, 21; 31, 54, 58}		12	8	7	7	6	2 (?)		8	5	7	3
{10, 26, 45; 15, 36, 40}	13	12	9	8		3	−1		8	7	2	−3
{11, 27, 46; 16, 37, 41}	11	9	5			10	7	3	8	5	6	3
{12, 28, 47; 17, 38, 42}		10	6			10	6	5	8	5	6	2
{13, 29, 48; 18, 39, 43}	13	12	9	8		2	0	−3	9 (?)	7	2	−3
{14, 25, 49; 19, 35, 44}	12	10	6			9	6	3	8	6 (?)	4	2

Table 6
Pariacoto virus: five-fold axial symmetric shells.

Radii and heights are in units of $d = R_0/12$.

	Capsid coat protein *A*								RNA chain *R*			
Decameric clusters	R_{pe}	R_e	R_i	R_{pi}	H_{pe}	H_e	H_i	H_{pi}	R_e	R_i	H_e	H_i
{0, 1, 2, 3, 4; 30, 31, 32, 33, 34}		11	7	4	10	8	5		5	3	8	7
{5, 17, 22, 41, 49; 12, 27, 35, 51, 59}	6	4	0			12	9	7	6	3 (?)	7 (?)	6
{6, 18, 23, 42, 45; 13, 28, 36, 52, 55}		11	8	6	8	7	4		8	5	6	2
{7, 19, 24, 43, 46; 14, 29, 37, 53, 56}	13	12	9	8	5	2	−2		9	7	2	−1
{8, 15, 20, 44, 47; 10, 25, 38, 54, 57}	13	12	9	8		5	1	0	9	7	2	−1
{9, 16, 21, 40, 48; 11, 26, 39, 50, 58}	12	11	8	7		7	4	2	8	5	6	2

5. Towards a physical interpretation: the resonator model

From the physical point of view, viral capsids exhibit a remarkable robustness, characterized by extreme elastic properties which ensure stability with respect to external forces and to the internal pressure of a densely packed genome. Experimentally, the mechanical properties of viral shells have been investigated by scanning force microscopy (Ivanovska *et al.*, 2004; Evilevitch *et al.*, 2011) and theoretically by normal mode analysis (Tama & Brooks, 2005; Peeters & Taormina, 2009; Klug *et al.*, 2006), by molecular dynamics calculations (Roos *et al.*, 2010; Zink, 2009) and by applying continuous elasticity theory (Bünemann, 2008). In the last two publications (which are PhD theses) one can find an extended list of references.

It is therefore natural to try to interpret the results presented in this paper in terms of elastic properties of the filled viral capsid. In doing so, the problem is to extract dynamical features from a purely geometric and static description of the viral structure.

The regular character of the shells described in terms of a set of equidistant spheres and cylinders suggests considering standing waves of eigenmode vibrations, in a capsid modeled

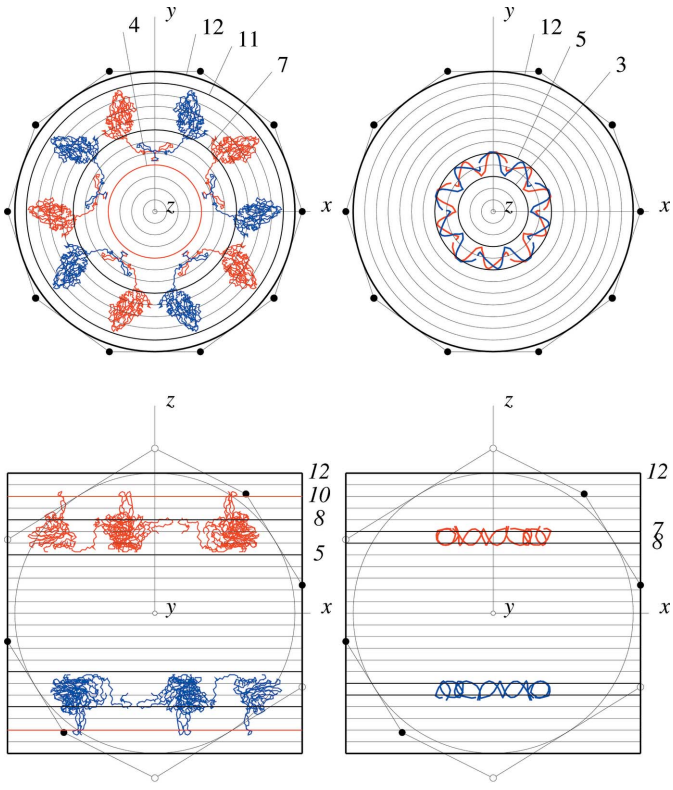

Figure 8
Plotted, in a similar way as in Fig. 7, are the axial shells formed by the five-fold pair of pentamers {0, 1, 2, 3, 4; 30, 31, 32, 33, 34} of the coat protein *A* (on the left-hand side) and of the RNA chain *R* (on the right-hand side) of the pariacoto virus, drawn in red and blue, respectively.

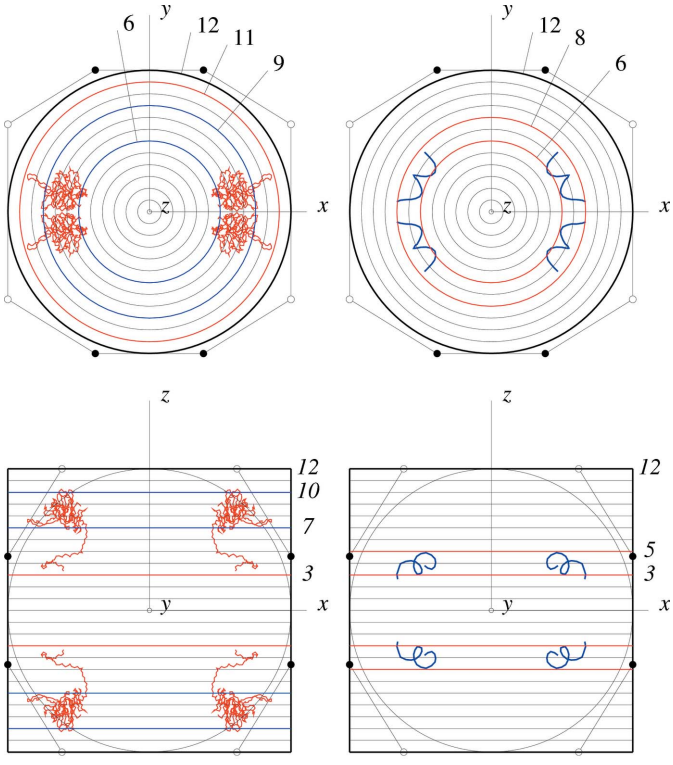

Figure 9
For the same pariacoto virus the shell structure of the coat protein *A* (red) and of the RNA chains *R* (blue) belonging to the tetramer {5, 24, 51, 56} are shown in a similar way as in Fig. 8.

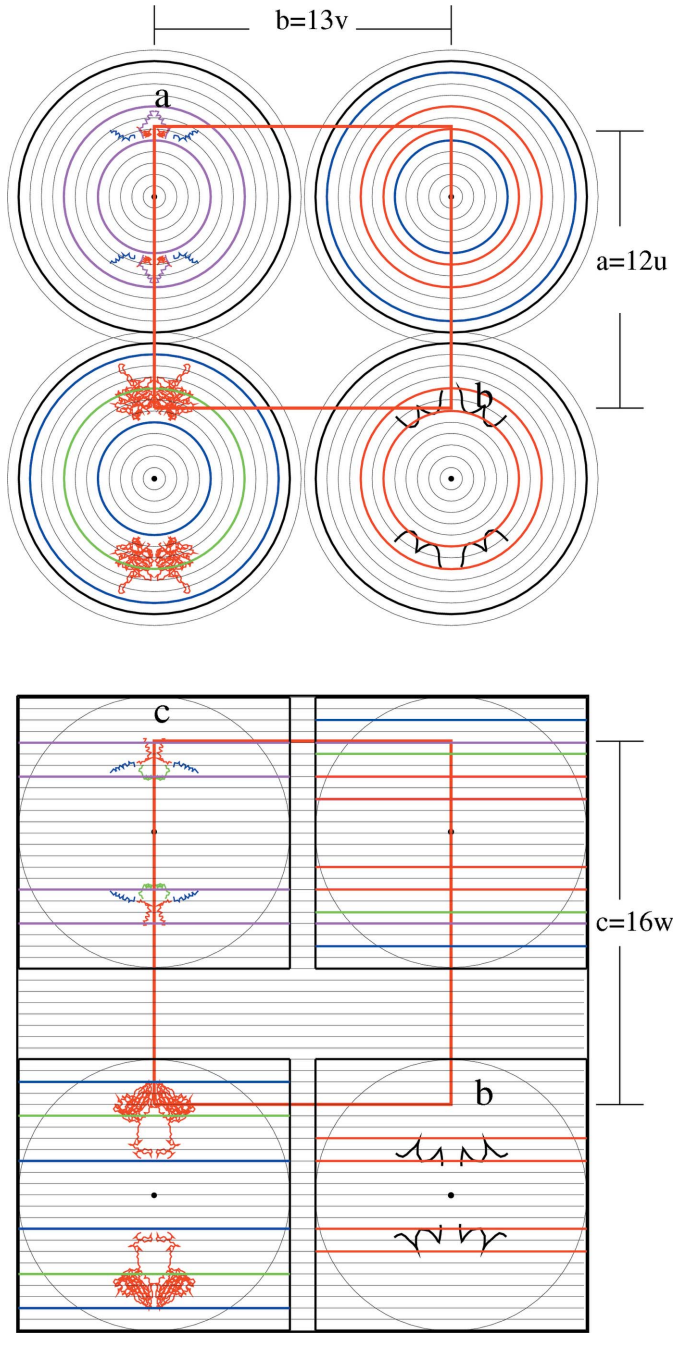

Figure 10
Compatibility between the axial shell structure and the crystal packing of the pariacoto virus in a projection along the crystal axis *c* and *a*, respectively. Shown in each of the projected views are the shell boundaries of the tetramer {5, 24, 51, 56}. Plotted in the bottom left are the β coat protein *A* (red), in the top left the γ coat proteins *D* (red), *E* (black), *F* (blue), and in the right views the RNA chain *R* (black). The various shell boundaries are also indicated in the two top right views.

as an elastic resonator, where the shells of the filled capsid build a kind of Chladni pattern, similar to those obtained by Ernst Chladni (1756–1827) from vibrating plates. In the general case of a finite elastic body, these patterns reveal vibrating eigenmodes which depend on boundary conditions. For a virus in the spherical approximation adopted, these conditions are those of the external (main) shell boundary of

Table 7
Nodal spherical surfaces.

	Capsid's shell centers				Genome's shell centers	
		Main shells	Protruded shells			
Virus	Chains	$(R_e + R_i)/2$	$(R_{pe} + R_e)/2$	$(R_{pi} + R_i)/2$	Chains	$(R_e + R_i)/2$
K_0 = 12-modes (radii in units of $d = R_0/K_0$)						
Cowpea	*A*, *B*, *C*	10.5			*D*, *F*	8.5
Tobacco	*A*	10.5		8.5	*B*, *C*	7.5
Pariacoto	*A*, *B*, *C*	10.5	12.5	8.5	*R*	8.0
	D	9.5				
	E, *F*	8.5				
MS2 phage					*S*	9.5
K_0 = 6-mode (radii in units of $2d = R_0/K_0$)						
MS2 phage	*A*, *B*, *C*	5.5			*R*	4.5

the capsid with radius R_e, which can be assumed to vibrate freely.

According to this interpretation, the shells of the various coat protein chains and of the RNA are delimited by anti-nodal surfaces, which for standing waves are equidistant: this implies, in particular, a wavelength λ equal to the inter-spacing distance d, of what can be denoted as a resonant K_0 = 12-mode. Nodal surfaces intercalate the anti-nodal ones. In this resonator model of the capsid the central region of each shell corresponds to the nodal surface of the resonant mode. It is in these regions that one expects to find (within a reasonable approximation) the centers of gravity of the chains, less affected by the vibrating eigenmodes, because they are in the nodal regions.

The shell boundaries of the four viruses have integral k values, as indicated in Table 2 for the spherical shells, and, in Tables 4, 5 and 6, integral k_R and k_H for the axial ones. It follows that the corresponding k values of nodal surfaces should be half-integers.

5.1. Vibrating spherical modes

The experimental situation observed for the spherical shells (main and protruded) of all the chains involved (proteins and RNA) is summarized in Table 7.

One finds indeed that the centers of the spherical shells of the cowpea chlorotic mottle virus and of the satellite tobacco mosaic virus are at nodal surfaces of the K_0 = 12 radial mode. This is also the case for the capsid shells of the pariacoto virus, but not for its genomic shell. Apparently the *R* chains which build the rigid dodecahedral RNA cage do not satisfy the assumption of enclosing freely vibrating boundaries, as required by anti-nodal surfaces.

In the case of the MS2 phage, only the boundaries of the RNA chains *S* are consistent with a K_0 = 12-mode. For all the other *A*, *B*, *C* and *R* chains it is for a resonant K_0 = 6-mode with wavelength $\lambda = 2d$ that one finds nodal surfaces (at the center of the spherical shells) with half-integer *k*-values.

5.2. Vibrating axial modes

As already remarked, the axial shells are less pronounced than the spherical ones, as one can see by comparing Table 2 with Tables 4, 5 and 6 for the pariacoto virus. Accordingly, a partial compatibility only is expected between the shell boundaries and anti-nodal surfaces of vibrating eigenmodes. As reported in Tables 8, 9 and 10 for the main shells of the coat protein *A* of the pariacoto virus, this is what one observes. One-third of the 62 different boundaries, in the rotation planes and in those perpendicular to the axis of the 31 axial clusters, do not have shell central regions with a half-integer k value of possible modes; the integral value found has been indicated together with a question mark. In general, those allowing an eigenmode interpretation are sub-harmonic of the fundamental K_0 = 12-mode and have a wavelength λ which is a multiple of d. These results confirm the secondary character of the axial modes with respect to the spherical ones.

The compatibility of the axial symmetric shells with the crystal structure is illustrated in Fig. 10 by the example of the {5, 24, 51, 56} tetrameric shells in the pariacoto virus by equidistant cylinders, in a similar way as by the array of equidistant spheres shown in Fig. 5 for the MS2 bacteriophage and in Fig. 6 for the cowpea chlorotic mottle virus. In general, the set of plane waves along the two-fold, three-fold and five-fold symmetry axes appear to be related to the spherical waves (with the same wavelength) as in diffraction phenomena.

5.3. Virus destruction by forced resonant oscillations

Capsid breaking and consequent viral destructions have been obtained by an osmotic shock (Anderson, 1950; Anderson *et al.*, 1953; Cordova *et al.*, 2003; Bünemann, 2008). The existence of resonant vibration modes in the filled capsid suggests breaking it and destructing the virus by forced resonant oscillations as an interesting alternative approach. It is a type of selective inactivation of viruses and bacteria which has been realised by applying femtosecond laser pulses (Tsen *et al.*, 2007, 2008, 2010). For interpreting this inactivation, a theoretical model of low-frequencies Raman spectra of icosahedral virus capsids has been developed by Dykeman & Sankey (2010). According to their calculations in the case of the satellite tobacco mosaic virus the resonant frequency is around 60–70 GHz. The present structural characterization of four viruses should allow the resonant approach to be refined and the selectivity of the method to be increased. Moreover, from the intimate relation between the virus and its crystal, one expects specific relations between the resonance frequencies of both systems. This opens even more possibilities in the fight against viral infections by purely physical methods, which will become more and more important because of the increasing viral resistivity against anti-viral drugs.

In any case, further theoretical and experimental investigations of these possibilities are justified.

Table 8
Nodal axial surfaces of the pariacoto capsid: two-fold axial shells of the coat protein *A*.

Radii and heights are in units of $\lambda = R_0/K_0$.

Clusters	Mode K_0	λ	$(R_e + R_i)/2$	Mode K_0	λ	$(H_e + H_i)/2$
{0, 32, 37, 46}	4	3*d*	3.5	3	4*d*	0.5
{1, 33, 38, 47}	4	3*d*	3.5	3	4*d*	0.5
{2, 34, 39, 48}	12	*d*	8.5	4	3*d*	2.5
{3, 30, 35, 49}	6	2*d*	2 (?)	4	3*d*	3.5
{4, 31, 36, 45}	12	*d*	8.5	4	3*d*	2.5
{5, 24, 51, 56}	4	3*d*	2.5	12	*d*	8.5
{6, 20, 52, 57}	12	*d*	9.5	12	*d*	2 (?)
{7, 21, 53, 58}	12	*d*	9.5	12	*d*	5.5
{8, 22, 54, 59}	4	3*d*	2.5	6	2*d*	4 (?)
{9, 23, 50, 55}	12	*d*	11 (?)	6	2*d*	0 (?)
{10, 15, 29, 43}	4	3*d*	3.5	6	2*d*	0.5
{11, 16, 25, 44}	12	*d*	11 (?)	3	4*d*	0.5
{12, 17, 26, 40}	12	*d*	5.5	12	*d*	9.5
{13, 18, 27, 41}	12	*d*	5.5	12	*d*	9 (?)
{14, 19, 28, 42}	4	3*d*	3.5	6	2*d*	0.5

6. Final remarks

New structural results could be obtained by applying, for the first time in virology, the inversion in a sphere. Most significant is the scale invariance of the properties derived in this way, properties which scale with the value of the radius R_0 of the invariant sphere. Of course, R_0, a transformation parameter only, does not represent an intrinsic property, which in fact depends on the value of the external radius R_e chosen to be equal to R_0 and considered as a measure of the viral size. This size appears to be a few percent smaller than the radius of the sphere enclosing the capsid adopted in previous publications. In the four viruses considered, this value varies from 85 Å to 155 Å, as indicated in Table 2, but the size does not affect their shared properties. The validity of a scaling principle has already been pointed out for the pariacoto virus by Wardman & Keef (2010); this poster is based on Keef *et al.* (2011) and other publications mentioned in the *Introduction*. The similarity of their work with the present one is due to the use of lattice-like structures (*Z*-modules, mathematically speaking) projected in space from six-dimensional lattices with icosahedral symmetry. The main difference is that scaling relations are obtained in the York approach of Twarock and her group by affine extension, whereas, in my own approach, scaling follows from non-Euclidean crystallographic transformations.

The geometrical shell model of the filled capsid and the dynamical one of the virus as a resonator allow the characterization of generic properties which suggest a common physical (and possibly biochemical) interpretation.

First of all, one finds a fairly clear separation between the globular quaternary structure of the coat proteins and a peripheral one consisting of loops and chain terminals which protrude the folded form. In terms of the shell model, one distinguishes accordingly between main and protruding shells. This characteristic morphology reflects the difference in the rôle played by these structural elements. As one knows, typical viral sites, like receptors, antigenic and binding sites are mostly localized on such external, and usually variable, chain segments, whereas the protruding elements directed towards the viral center are responsible for the interaction between capsid and genome.

The strong elastic properties of the capsid, required by the protecting rôle of this envelope, depend on the value of typical shell parameters, like the width (Bünemann, 2008), which in the shell model appears as the radial difference $R_e - R_i$ of the external and the internal boundary. In the genome, similar shell regions delimit the ordered RNA parts which fit with the overall icosahedral symmetry of the virus, and whose atomic coordinates could, therefore, be determined by X-ray diffraction.

Concluding, the shell model adopted reflects, in a natural way, typical viral properties.

One additional property of these shells, that to have boundaries fitting with an equidistant array of spherical surfaces and cylindrical ones, leads to the resonator model represented by an elastic sphere having its own resonant modes of standing waves, with anti-nodal surfaces fitting with the boundaries of the various shells. One finds that the wavelengths of the eigenmodes are a multiple of a fundamental one λ_0 equal to the equidistant inter-spacing d, with $d = R_0/12$, where R_0 is the radius of the invariant

Table 9
Nodal axial surfaces of the pariacoto capsid: three-fold axial shells of the coat protein *A*.

Radii and heights are in units of $\lambda = R_0/K_0$.

Clusters	Mode K_0	λ	$(R_e + R_i)/2$	Mode K_0	λ	$(H_e + H_i)/2$
{0, 9, 22; 32, 50, 59}	12	*d*	5 (?)	3	4*d*	2.5
{1, 5, 23; 33, 51, 55}	12	*d*	5.5	12	*d*	9 (?)
{2, 6, 24; 34, 52, 56}	4	3*d*	3.5	12	*d*	6.5
{3, 7, 20; 30, 53, 57}	12	*d*	11 (?)	6	2*d*	0 (?)
{4, 8, 21; 31, 54, 58}	3	4*d*	2.5	6	2*d*	8 (?)
{10, 26, 45; 15, 36, 40}	4	3*d*	3.5	12	*d*	2 (?)
{11, 27, 46; 16, 37, 41}	12	*d*	7 (?)	12	*d*	8.5
{12, 28, 47; 17, 38, 42}	6	2*d*	4 (?)	6	2*d*	4 (?)
{13, 29, 48; 18, 39, 43}	4	3*d*	3.5	6	2*d*	0.5
{14, 25, 49; 19, 35, 44}	6	2*d*	4 (?)	4	3*d*	2.5

Table 10
Nodal axial surfaces of the pariacoto capsid: five-fold axial shells of the coat protein *A*.

Radii and heights are in units of $\lambda = R_0/K_0$.

Clusters	Mode K_0	λ	$(R_e + R_i)/2$	Mode K_0	λ	$(H_e + H_i)/2$
{0, 1, 2, 3, 4; 30, 31, 32, 33, 34}	12	*d*	9 (?)	12	*d*	7 (?)
{5, 17, 22, 41, 49; 12, 27, 35, 51, 59}	3	4*d*	0.5	4	3*d*	3.5
{6, 18, 23, 42, 45; 13, 28, 36, 52, 55}	12	*d*	9.5	12	*d*	5.5
{7, 19, 24, 43, 46; 14, 29, 37, 53, 56}	4	3*d*	3.5	6	2*d*	0 (?)
{8, 15, 20, 44, 47; 10, 25, 38, 54, 57}	4	3*d*	3.5	12	*d*	3 (?)
{9, 16, 21, 40, 48; 11, 26, 39, 50, 58}	12	*d*	9.5	12	*d*	5.5

sphere and corresponds to the size of the virus. The origin of the numeric value 12, observed in all four viruses, is unknown. Here, it is accepted as empirically fact. Usually the detection of eigenvibrations allows the matter distribution inside the given sphere to be deduced. In the present approach the converse idea is applied.

It is worthwhile being aware that the idea of viral destruction by forced resonant oscillations has not been simply taken over from other investigations, like the pioneering ones of the Tsens and co-workers, but it represents the follow up of a series of purely geometrical studies of crystallographic properties of biomacromolecules. At present one can barely imagine all possible consequences of the physical interpretation of these properties; the number of different biomacromolecules is too large.

APPENDIX *A*
Comments on obtaining the results

A1. Graphical fitting

The existence of equally spaced shells in the four RNA viruses considered, which represents the main result of the paper, has been obtained by a two-dimensional graphical fitting between the images of the real structure (in the C_α backbone approximation of the proteins and in the P-backbone one of the RNA chains) and the geometry of an ideal viral model. The question then arises whether this basic property is not an artefact of the fitting procedure which has been carried out by eye.

Let me first note that a change in precision of the fitting procedure within reasonable limits only modifies the shell parameters of the real structure (which anyway is only approximately known) but not those of the ideal one.

The graphical procedure adopted in this paper (and in most of the previous publications on biomacromolecules) for obtaining a two-dimensional image from a three-dimensional object is a *projection* and neither a section nor a stereo diagram.

Projection is particularly suited to spherical objects. The radius of the sphere is equal to the radius of its projected circle. In the spherical approximation of an icosahedral virus, one then directly read out in the projected image the radius of the external enclosing form; not, however, that of an internal spherical boundary. This is the reason why one first inverts the virus and then projects it. Knowing the radius of the invariant sphere (and this is easily done if one takes for it the external boundary as explained above) one then deduces from the projected inverted image the value of the internal radius. Putting equal to 1 the radius of the invariant sphere, the relation between the internal radius R_i and of that of the projected image R_p is simply $R_i = 1/R_p$. This relation is independent of the special choice mentioned above, where the surface of the spherical virus is taken as invariant under the inversion considered.

The situation is slightly different in the case of axial-symmetric shells, which are claimed to be equally spaced cylindrical surfaces, because the circular shell boundaries (the only relevant ones for the resonator model) are invariant under projection in the axial direction. Modified by this projection are only the axial-symmetric set of the chains, as indicated in Figs. 7–10.

The property used in these graphical fittings is that the points which have an extremal radial distance from the axis conserve this property in their two-dimensional image. The validity of the periodic shell characterization (which involves these extremal points) is directly visible from the images and does not need further comments about its reality, which in the biological structure is only an approximation and whose relevance has still to be tested. The question marks appearing in Tables 4, 5 and 6 concern deviations relevant only for the interpretation of the shell boundaries as nodal and anti-nodal regions in the resonant model.

A2. Inversive geometry

In the graphical fitting, use has been made for the various viruses considered of the inversion in a sphere. The new question is whether this procedure is universal and can be applied to any virus.

Inversion in a sphere is indeed a universal procedure belonging to the *inversive geometry*, which can be defined for arbitrary dimensions and includes the Euclidean geometry as a special case (with the centers of the spheres at infinity). Euclidean repeated reflections on two parallel planes generate translations. These correspond to scalings obtained by combined inversions on two concentric invariant spheres. Rotations are conserved under inversion, up to their orientation (Coxeter, 1961), so that the point group symmetry (and in particular the icosahedral symmetry) is conserved.

Not conserved under inversion are the non-spherical forms, like the polyhedral and the polygonal forms. For example, the icosahedron is not transformed into an icosahedron, as, in general, plane facets are mapped into rounded ones.

Inversion can thus be applied to any virus. One can always obtain as external an internal form. But, in order to correctly interpret the form obtained, one has to know how the two are related. This aspect is of particular importance if one applies inversion to the Caspar–Klug viral characterization.

A3. Biology of periodic shell arrangements

The above considerations are intended to show that the periodic shell arrangements are not artefacts of the fitting procedure, but represent real facts, at least in the ideal case. The following question is whether this construction, if not a perfect description it, is still a good approximation of the biology.

Shell structures in viruses have been observed and discussed by quite a number of other investigators (see *e.g.* Bünemann, 2008), to begin with the separation between capsid and genome. Periodicity is the new result which justifies the publication of the present paper. The biological foundation for such an arrangement depends on the interpreted physical properties.

In the resonator model, the assignment of nodal positions to the approximate center of gravity of the chains, and of anti-nodal positions to their boundaries minimizes the kinetic energy of the vibrational modes. Indeed a large amplitude movement there where one finds most of the mass distribution would require more kinetic energy.

The paper only considers static structural properties and not dynamical ones. This is the reason why the resonator model adopted is based on a Chladni-like figure interpretation of the observed chain distribution, allowing the gap between statics and dynamics to be bridged. Limitations of this characterization have to be taken into account. In particular, Chladni figures of resonating plates are revealed by fine powders, and are not obtained from chain-like elements as considered in the present case. Therefore, deviations between Chladni-like patterns and viral chain distributions (indicated by question marks in Tables 4 to 6 and 8 to 10, and which only concern axial-symmetric shells) are not a serious counter-indication.

Suppose now that the resonant model is not the correct interpretation of the chain periodicity. As an alternative, one could argue that a spherical periodic arrangement of coat proteins, involving successive chain parts with different bindings, can ensure to the capsid stronger mechanical (elastic) properties (which are extreme) in a similar way as in plywood. The plywood model is more questionable for the RNA part, and it is not so natural for the axial-symmetric shells.

In fact, only experimental investigations (which I hope should start soon at the university of Nijmegen as well) will allow the validity of a biological interpretation in terms of a given physical model to be tested.

The relevance of forced oscillations leading to a capsid instability has already been established by other research groups. Independently of the resonator or of the plywood model, knowledge of the intriguing structural features presented should allow a better understanding of the viral properties.

References

Anderson, T. F. (1950). *J. Appl. Phys.* **21**, 70.

Anderson, T. F., Rappaport, C. & Muscatine, N. A. (1953). *Ann. Inst. Pasteur*, **84**, 5–14.

Bünemann, M. (2008). PhD Thesis, Philipps-University, Marburg, Germany.

Cordova, A., Deserno, M., Gelbart, W. M. & Ben-Shaul, A. (2003). *Biophys. J.* **85**, 70–74.

Coxeter, H. S. M. (1961). *Introduction to Geometry*, pp. 77–95. New York: John Wiley.

Dykeman, E. C. & Sankey, O. F. (2010). *Phys. Rev. E*, **81**, 021918.

Evilevitch, A., Roos, W. H., Ivanovska, I. L., Jeembaeva, M., Jönsson, B. & Wuite, G. J. (2011). *J. Mol. Biol.* **405**, 18–23.

Grayson, N. E., Taormina, A. & Twarock, R. (2009). *Theor. Comput. Sci.* **410**, 1440–1447.

Guérin, Th. & Bruinsma, R. (2007). *Phys. Rev. E*, **76**, 061911.

Ivanovska, I. L., de Pablo, P. J., Ibarra, B., Sgalari, G., MacKintosh, F. C., Carrascosa, J. L., Schmidt, C. F. & Wuite, G. J. L. (2004). *Proc. Natl Acad. Sci. USA*, **101**, 7600–7605.

Janner, A. (2004). *Acta Cryst.* A**60**, 198–200.

Janner, A. (2005*a*). *Acta Cryst.* D**61**, 247–255.

Janner, A. (2005*b*). *Acta Cryst.* D**61**, 256–268.

Janner, A. (2005*c*). *Acta Cryst.* D**61**, 269–277.

Janner, A. (2008). *Acta Cryst.* A**64**, 494–502.

Janner, A. (2010*a*). *Acta Cryst.* A**66**, 301–311.

Janner, A. (2010*b*). *Acta Cryst.* A**66**, 312–326.

Janner, A. (2011*a*). *Acta Cryst.* A**67**, 517–520.

Janner, A. (2011*b*). *Acta Cryst.* A**67**, 174–189.

Jonoska, N. & Twarock, R. (2006). arXiv: q-bio/0611021v1.

Keef, T. & Twarock, R. (2009*a*). *J. Math. Biol.* **59**, 287–313.

Keef, T. & Twarock, R. (2009*b*). *Emerging Topics in Physical Virology*, edited by P. G. Stockley & R. Twarock, pp. 59–84. London: Imperial College Press.

Keef, T., Wardman, J., Ranson, N. A., Stockley, P. C. & Twarock, R. (2011). *PLoS Biol.* Submitted.

Klug, W. S., Bruinsma, R. F., Michel, J.-P., Knobler, Ch. M., Ivanovska, I. L., Schmidt, Ch. F. & Wuite, G. J. L. (2006). *Phys. Rev. Lett.* **97**, 228101.

Larson, S. B., Day, J., Greenwood, A. & McPherson, A. (1998). *J. Mol. Biol.* **277**, 37–59.

Peeters, K. & Taormina, A. (2009). *J. Theor. Biol.* **256**, 607–624.

Roos, W. H., Gibbons, M. M., Arkhipov, A., Uetrecht, C., Watts, N. R., Wingfield, P. T., Steven, A. C., Heck, A. J., Schulten, K., Klug, W. S. & Wuite, G. J. (2010). *Biophys. J.* **99**, 1175–1181.

Speir, J. A., Munshi, S., Wang, G., Baker, T. S. & Johnson, J. E. (1995). *Structure*, **3**, 63–78.

Stockley, P. G. & Twarock, R. (2009). Editors. *Emerging Topics in Physical Virology*, p. 332. London: Imperial College Press.

Tama, F. & Brooks, C. L. (2005). *J. Mol. Biol.* **345**, 299–314.

Tang, L., Johnson, K. N., Ball, L. A., Lin, T., Yeager, M. & Johnson, J. E. (2001). *Nat. Struct. Biol.* **8**, 77–83.

Toropova, K., Basnak, G., Twarock, R., Stockley, P. G. & Ranson, N. A. (2008). *J. Mol. Biol.* **375**, 824–836.

Tsen, K. T., Tsen, S.-W. D., Hung, C.-F., Wu, T.-C. & Kiang, J. G. (2008). *J. Phys. Condens. Matter*, **20**, 252205.

Tsen, K. T., Tsen, S.-W. D., Sankey, O. F. & Kiang, J. G. (2007). *J. Phys. Condens. Matter*, **19**, 472201.

Tsen, S.-W. D., Tsen, Y.-S. D., Tsen, K. T. & Wu, T. C. (2010). *J. Healthcare Eng.* **1**, 185–196.

Valegård, K., Murray, J. B., Stonehouse, N. J., van den Worm, S., Stockley, P. G. & Liljas, L. (1997). *J. Mol. Biol.* **270**, 724–738.

Wardman, J. & Keef, T. (2010). *3rd Mathematical Virology Workshop*, Ambleside, UK. Poster.

Zink, M. (2009). PhD Thesis, pp. 156, Georg-August-University, Göttingen, Germany.